Agricultural Water Management 274 (2022) 107965

Contents lists available at ScienceDirect

Agricultural Water Management

journal homepage: www.elsevier.com/locate/agwat

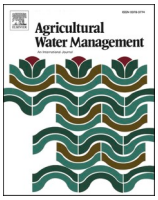

Remote sensing-based evapotranspiration modeling using geeSEBAL for sugarcane irrigation management in Brazil

I.Z. Gonçalves [a,*], A. Ruhoff [b], L. Laipelt [b], R.C. Bispo [c], F.B.T. Hernandez [c], C.M.U. Neale [d], A.H.C. Teixeira [e], F.R. Marin [a]

[a] University of São Paulo (USP), "Luiz de Queiroz" College of Agriculture (Esalq), Piracicaba, SP, Brazil
[b] Institute of Hydraulic Research - Federal University of Rio Grande do Sul, Brazil
[c] São Paulo State University – UNESP, Brazil
[d] University of Nebraska, Daugherty Water for Food Global Institute, United States
[e] Federal University of Sergipe, Brazil

ARTICLE INFO

Handling Editor - Dr. B.E. Clothier

Keywords:
Water productivity
Landsat images
ERA5
Eddy covariance

ABSTRACT

Irrigated agriculture requires the implementation of innovative tools to improve irrigation water management and accurate estimation of actual evapotranspiration (ETa) such as remote sensing-based methodology. This study aimed to evaluate the irrigation management and estimating evapotranspiration through the geeSEBAL, a new tool for automated estimation of ETa based on the Surface Energy Balance Algorithm for Land (SEBAL) and a simplified version of the Calibration using Inverse Modeling at Extreme Conditions (CIMEC) process for the endmembers selection, implemented into the Google Earth Engine (GEE) environment. GeeSEBAL has not been used yet in Brazil for irrigation proposes, and in this research, it was applied to estimate ETa using Landsat images and ERA5-Land as meteorological inputs in the largest sugarcane producing region of the world in Brazil for two ratoon seasons by comparing daily ETa with values obtained from eddy covariance (EC) data, Energy balance components using geeSEBAL were consistent with the measured data and daily ETa presenting RMSE of 0.46 mm with $R^2 = 0.97$. Modeled ETa and Kc were similar for the two seasons, although somewhat over-estimated for the fifth ratoon when compared to the EC data, mainly during high atmospheric demand (crop mid-stage). Still, the Kc values were similar to the standard values available in the literature and measured flux tower data for the two ratoons seasons. With ETa from geeSEBAL it was possible to identify water stress over the growing seasons using the remote sensing-based soil water balance, which occurred mainly during the phase after the crop reached the peak Kc (full cover stage) when the irrigation depth required was very high. This analysis showed that geeSEBAL has a significant potential for assessment of ETa for irrigation monitoring and management, even in missing climate data areas, allowing important advances in water resources management for sugarcane and other irrigated crops at field or regional scales.

1. Introduction

Rapid population growth has increasingly raised concerns in the global community about the role of agricultural production on the high demand for food and its impact on ecosystem sustainability. According to PRB - Population Reference Bureau (2020), the global population will reach almost 10 billion people in 2050, and food production is expected to increase by 35–56% to meet the demand (Dijk et al., 2021). Tropical climate countries with an extensive territorial area such as Brazil are well known as important global food producers and exporters, serving as a key supplier of food and other commodities such as fiber and biofuels. However, even in large countries, agricultural lands are limited, and water resources are increasingly scarce due to climate extremes.

Although Brazil is the world's largest sugarcane producer with an estimated production of more than 650 million tons in 8.6 million hectares, most sugarcane fields are under rainfed conditions, and the average yield is around 69 Mg ha^{-1} (CONAB, 2021). To overcome low yields and increase efficiency in land use to boost food security, irrigation practices have been adopted and the expansion rate of irrigation has grown in the country.

* Corresponding author.
E-mail address: ivo.zution@gmail.com (I.Z. Gonçalves).

https://doi.org/10.1016/j.agwat.2022.107965
Received 9 July 2022; Received in revised form 22 September 2022; Accepted 23 September 2022
Available online 21 October 2022

For irrigation management, satellite images provide an excellent means for determining and mapping the spatial and temporal ETa, having great potential for improving irrigation management, by providing ETa estimations for large land surface areas using a minimal amount of ground data. Some recent studies have used remote sensing (RS) models successfully to monitor and improve irrigation management worldwide (Campos et al., 2016; Campos et al., 2018; Venancio et al., 2019; Foster et al., 2019).

The choice of an ETa model depends on several factors, including the type of application, spatial and temporal resolutions, meteorological inputs, and the expected model advantages and limitations (Zhang et al., 2016). RS-based methodologies for estimating ETa can be separated into two main groups: (1) vegetation indexes-based models, where ETa is estimated based on the basal crop coefficient as a function of the spectral reflectance values (Neale et al., 1989) derived from vegetation indexes such as Land Surface Evapotranspiration (MOD16) (Mu et al., 2011), and (2) land surface temperature-based models, based on the energy balance approach; these models can be one source when ETa is estimated for soil and vegetation together as a single layer such as the well-known SEBAL (Bastiaanssen et al., 1998a) and METRIC (Allen et. al, 2007), and two sources when ET is estimated for soil and vegetation individually such as the Two Source Energy Balance (TSEB) (Norman et al., 1995), and ALEX-DisALEX model (Anderson et. al, 1997, Mecikalski et. al, 1999; Norman et al., 2003). Yet, these models use orbital imagery and ground-based meteorological data, and depending on the model, can also use field data to estimate the components of the energy balance (latent and sensible heat, and soil heat flux) and ETa.

Among several surface temperature (Ts)-based models, SEBAL computes ETa from satellite images and weather data using the surface energy balance and has been successfully applied worldwide across different climates and land cover conditions for water resources management presenting accurate results (Bastiaanssen et al., 2005; Bhattarai et al., 2012; Ruhoff et al., 2012; Tang et al., 2013; Wagle et al., 2017; Yang et al., 2012). The main component of the algorithm is the internal process to estimate the near-surface temperature gradient (dT), which is based on the selection of endmembers that represent the extremes of the wet (cold) and dry (hot) ETa spectrum (Allen et al., 2007; Bastiaanssen et al., 1998a). While this was manually performed in early applications, an algorithm based on surface temperature and normalized deviation vegetation index (NDVI) percentiles using the Calibration Inverse Modeling at Extreme Conditions (CIMEC) has allowed the automatic selection of endmember candidates pixels (Allen et al., 2013). This algorithm enabled the use of multiple images within a fully automated ETa framework, improving and facilitating the assessment of time series based on RS images (Bhattarai et al., 2017; Jaafar and Ahmad, 2019). Considering the importance of estimating ET worldwide for water resources management, even in isolated areas where ground data is not available such as automatic weather station to provide meteorological data, this might be a critical aspect that can be overcome using an open-source SEBAL framework implemented within the Google Earth Engine (GEE) through application programming interface (API), named geeSEBAL (Laipelt et al., 2021).

Reflecting the importance of accurate ETa estimates for irrigation monitoring and management through remote sensing, even in areas where meteorological data is scarce, the main goals of this study was to use an open-source SEBAL framework implemented into Google Earth Engine (GEE - https://earthengine.google.com/) through API, known as geeSEBAL, to estimate temporal and spatial ETa, RS-crop development, crop coefficient (Kc), and RS-based soil water balance (RS-SWB) over two sugarcane growing seasons (two years) grown in the northwest state of São Paulo, Brazil using current Landsat 8 (OLI) and Landsat 7 (ETM+) images, and the state-of-the-art meteorological reanalysis from ERA5-Land. This approach has not been used in Brazil yet for irrigation proposes in sugarcane, and could be a great initiative to encourage the researcher community to use remote sensing technique with only orbital data without using meteorological inputs from terrestrial data to estimate the energy balance components and ET collaborating with the advance in monitoring the crop water management. Additionally, an evaluation of the performance results of the estimated energy balance (EB) components and ETa using geeSEBAL against field data obtained from the turbulent flux data (Eddy Covariance) was conducted.

2. Material and methods

2.1. Study site

This research was carried out in a commercial field of 24 ha in the western state of São Paulo (latitude 20°43'43.6″ S, longitude 51°16'30.3″ O), 360 m above sea level (Fig. 1), grown with sugarcane for two ratoon seasons, fourth and fifth harvesting seasons, respectively (June 2016 to June 2018), with the variety RB96–6928. The research site is located in the largest sugarcane producing region in the world, representing more than 90% of all Brazilian production (CONAB, 2021).

According to the Koppen classification (Peel et al., 2007), the climate of the region is defined as tropical type (Aw) with dry winter and rainy summer, with average annual precipitation of 1.242 mm, average annual reference evapotranspiration of 1536 mm, average solar radiation of 17 MJ m^{-2} day^{-1}, average air temperature of 23° C, and average relative humidity of 62% (UNESP, 2019). The soil is classified as Typical Dystrophic Red Latosol (Santos et al., 2018), deep with sandy loam texture, more details about the soil's physical characteristics are in Bispo et al. (2022) and Table 1.

The meteorological data used were collected from the automated weather station (Northwestern São Paulo Network - http://clima.feis.unesp.br) near the study site, and used to estimate the reference evapotranspiration (ETo) based on the FAO-Penman-Monteith method (Allen et al., 1998).

Planting was done in September 2013 (first harvest) with single rows spaced at 0.9 m apart and 1.5 m between double rows. The crop was irrigated using a subsurface drip irrigation system with the drip tapes buried at 0.40 m depth, supplying a flow rate of 1 L $hour^{-1}$ per dripper spaced 0.6 m apart.

2.2. Google earth engine application: the geeSEBAL algorithm

SEBAL estimates ETa based on thermal and multispectral remote sensing datasets that calculate latent heat flux (LE) as a residual by subtracting the soil heat flux and sensible heat flux from the net radiation (Rn) of the instantaneous surface energy balance equation (Eq. (1)). LE is the energy used to convert liquid water into water vapor, i.e., evapotranspiration. More details about SEBAL model formulation and calibration are well documented in Laipelt et al. (2021), Bastiaanssen et al. (1998a) and Bastiaanssen et al. (1998b).

$$LE = Rn - G - H \tag{1}$$

where LE is the latent heat flux (W/m^2); Rn is the net radiation; G: is the soil heat flux (W/m^2); H is the sensible heat flux (W/m^2).

$$\wedge = \frac{LE}{Rn - G} \tag{2}$$

Where $\wedge$ is the evaporative fraction; LE is the latent heat flux (W/m^2); Rn is the net radiation (W/m^2); G is the soil heat flux (W/m^2).

To estimate G, we used a calibrated equation a function locally fitted from NDVI and albedo (Eq. (3)).

$$\frac{G}{R_n} = T_s(0.015 \quad \alpha)(1 - 0.8 \quad NDVI^{1/3} \quad) \tag{3}$$

Where G is the soil heat flux (W/m^2); Rn is the net radiation (W/m^2); Ts is the surface temperature (°C); α is the albedo; NDVI is the normalized difference vegetation index.

The evaporative fraction (Λ) (Eq. (2)) is computed by upscaling

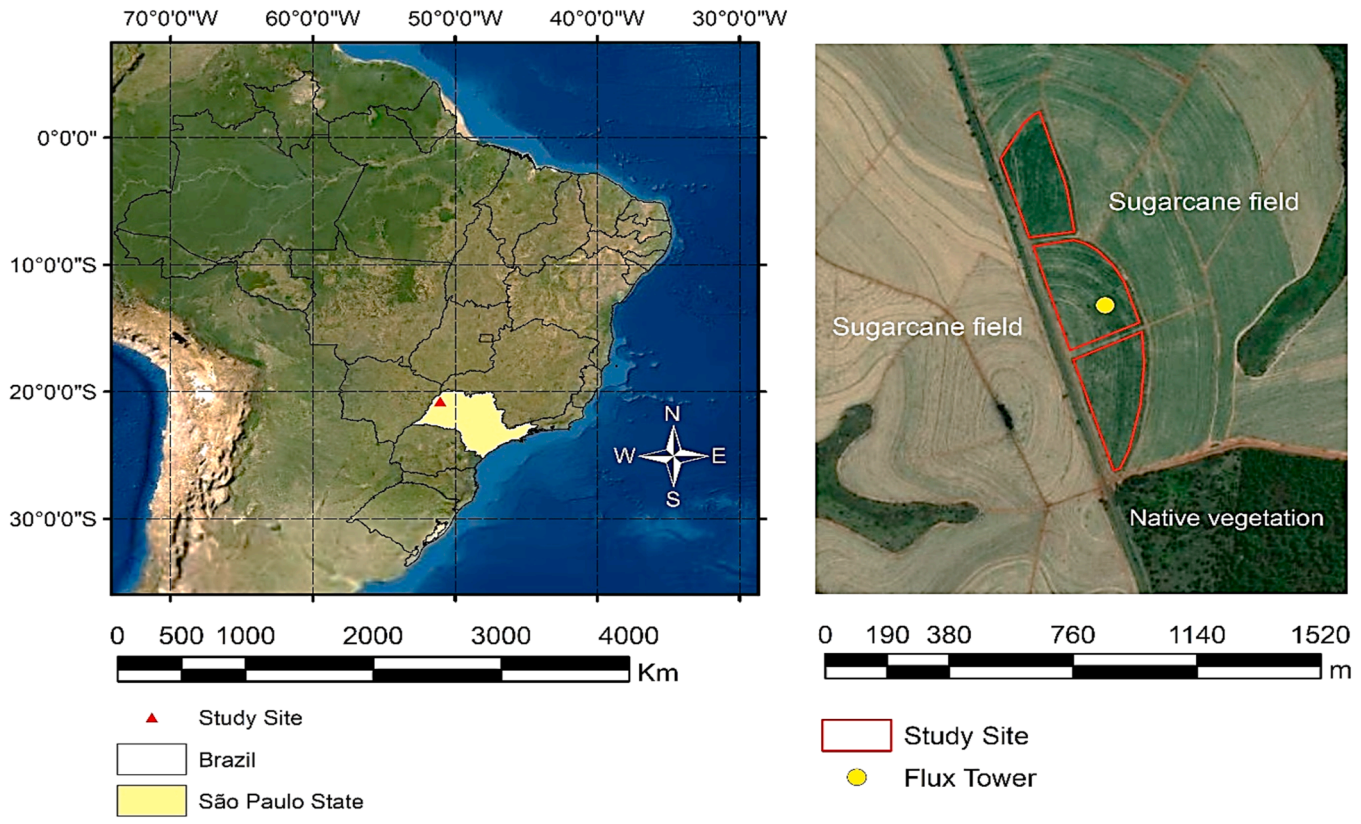

Fig. 1. Location of the study site in the western State of São Paulo - Brazil (left) and sugarcane field and surroundings (right).

Table 1
Physical characteristics of the soil profile for each 0.20 m layer deep for the study site.

Layer (m)	Sand (%)	Silt (%)	Clay (%)	Field capacity (m m^{-1})	Wilting point (m m^{-1})	1BD (g cm^{-3})	[2]TAW (mm)
0–0.20	76.4	10.6	13.0	0.16	0.057	1.60	33.0
0.20–0.40	75.6	8.40	16.0	0.17	0.072	1.64	32.1
0.40–0.60	72.8	7.10	20.1	0.15	0.058	1.58	29.0
Average	74.9	8.7	16.4	0.16	0.062	1.61	31

1BD: bulk density; [2]TAW: total available water.

instantaneous LE to daily ETa (i.e., $ETa_{24\,h}$) (Eq. (4)).

$$ETa_{24h} = \frac{\wedge Rn_{24h}}{\lambda} \quad (4)$$

Where $ETa_{24\,h}$ is the daily evapotranspiration (mm); $Rn_{24\,h}$ is the daily average net radiation (W/m^2); $\wedge$ is the evaporative fraction; λ is the latent heat of vaporization of water (J/Kg).

The SEBAL algorithm was implemented into GEE (geeSEBAL - version 0.1.217) using the JavaScript and Python APIs (Laipelt et al., 2021). GEE provides the entire Landsat collection and hourly ERA5-Land data, allowing geeSEBAL processing to be applied in different regions of the globe with high-performance computing, even in regions where ground meteorological data is totally limited. The geeSEBAL tool has three main functions: Image: estimation of ETa from a specific image (available for JavaScript and Python); ImageCollection: batch process to estimate ETa given a date period (exclusive for Python); TimeSeries: estimation of ETa time series over long-term periods at user-provided coordinates (exclusive for Python). All codes and applications are freely available at https://github.com/et-brasil/geesebal. A graphical user interface version of geeSEBAL also is available through an Earth Engine application (https://etbrasil.org/geesebal) and for more detail about the geeSEBAL tool, we suggest Laipelt et al. (2021) and Kayser et al. (2022). A flow chart of geeSEBAL showing the step-by-step processing to estimate daily ET and validation is presented in Fig. 2.

Input image data used to run geeSEBAL was the atmospherically corrected land surface reflectance and brightness temperature image collection from Landsat 8 Operational Land Imager (OLI)/Thermal Infrared Sensor (TIRS) and Landsat 7 Enhanced Thematic Mapper Plus (ETM+), Path/Row 222/74 and 223/74 with cloud-free images from June 2016 to June 2018, with the highest data quality available (Tier 1). A total of 77 images were used. Cloud cover filters from the CFMask algorithm (Foga et al., 2017) were used to identify clouds and shadows pixels for each image. For global instantaneous meteorological inputs, we used data from the ERA5-Land reanalysis dataset (Hersbach et al., 2020; Munoz-Sabater et al., 2021) at the hourly temporal resolution, including air temperature at 2 m (Tair), dew point temperature (Tdew) and eastward and northward wind speed at 2 m at the time of Landsat satellite overpass. Relative humidity (RH) was estimated following Shuttleworth (2012).

Land surface temperature (LST) was adjusted to a common elevation datum (Tsdem) using digital elevation data from the Shuttle Radar Topography Mission (SRTM), considering an average lapse rate of 6.5° C km^{-1}, and slope effects also were corrected, according to Jaafar and Ahmad (2019).

Time-series soil-adjusted vegetation index, known as SAVI (Vermote et al., 2016; Masek et al., 2006), was used according to Eq. (5) to

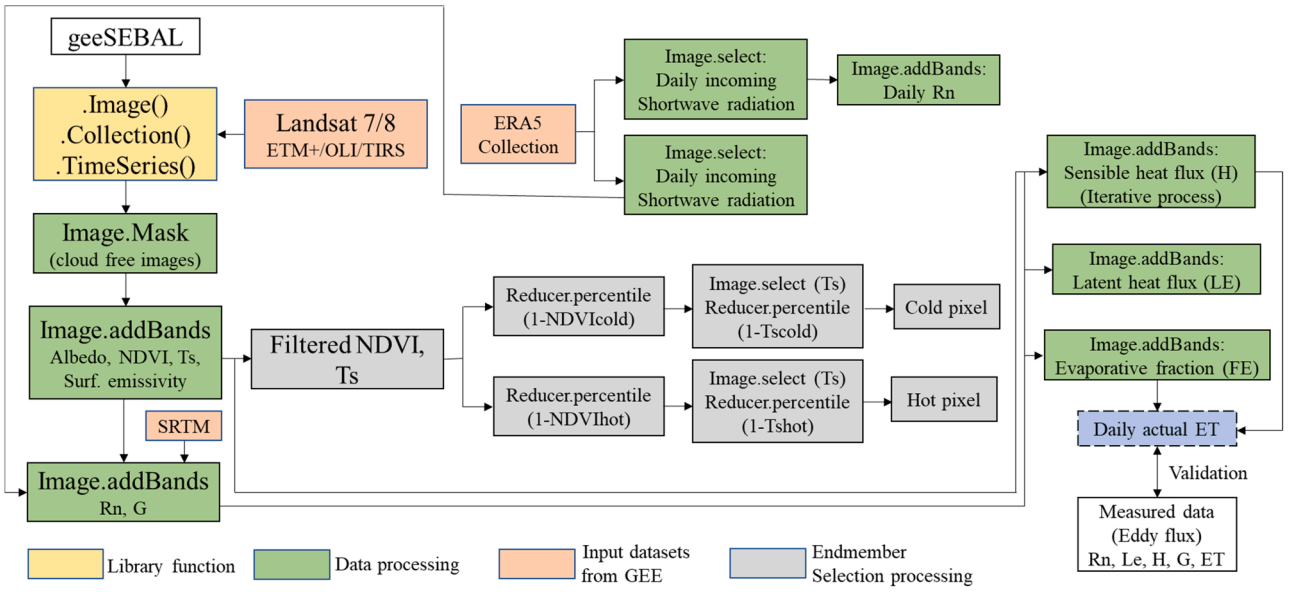

Fig. 2. Flow chart of geeSEBAL demonstrating remote sensing, meteorological inputs and GEE functions for data processing to estimate daily evapotranspiration.

monitor the two sugarcane ratoons' development. SAVI is an index designed to mitigate changing soil background effects on analyzed images if the land surface is not fully covered by vegetation, highly recommended in irrigated areas.

$$SAVI = \frac{NIR + RED}{NIR - RED + L} * (1 + L) \quad (5)$$

Where SAVI is the soil-adjusted vegetation index; NIR is the reflectance value of the near red band (0.845–0.885 μm; 30 m resolution); RED is the reflectance value of the red band (0.630–0.680 μm; 30 m resolution); L is the soil cover coefficient by green vegetation, value = 0.5.

2.3. geeSEBAL remote sensing and meteorological data

Inputs such as atmospherically corrected land surface reflectance and brightness temperature image collection from Landsat 7 and 8 (Tier 1) was used to run geeSEBAL. Also, it was implemented cloud cover filters from the CFMask algorithm for each image (Foga et al., 2017) to improve the image quality. For global meteorological inputs, we used data from the ERA5-Land reanalysis dataset (Hersbach et al., 2020; Munoz-Sabater et al., 2021) at hourly data, including air temperature at 2 m (Tair), dew point temperature (Tdew) and eastward and northward wind speed at 10 m (u), at the time of Landsat satellite overpass. About the estimation of relative humidity (RH), we followed Shuttleworth (2012). ERA5-Land was selected mainly due to its global coverage and high spatial and temporal resolution when compared to other reanalysis data available in GEE.

Additionally, we used incoming shortwave radiation data (global radiation), aggregated at daily time step. Furthermore, the digital elevation model from SRTM was also used for the Ts correction.

2.4. Hot and cold endmembers: automated calibration

The automated statistical algorithm to select the hot and cold endmembers is based on a simplified version of the CIMEC algorithm used in METRIC (Allen et al., 2013), subsequently evaluated by Morton et al. (2013), where percentiles of LST and normalized difference vegetation index (NDVI) values are used to select endmember candidates. The CIMEC procedure is used to calibrate the dT function of Eq. (2). The CIMEC process is applied by inverting Eq. (6) for dT after solving Eq. (1) for H for the two extreme endpoint conditions in the image representing nearly full LE (cold endmember) and nearly zero LE (hot endmember).

$$H = \frac{pc_p dT}{r_{ah}} \quad (6)$$

Where q is air density (kg/m^3), cp is air specific heat, (J/kg/K), dT (K) is the temperature difference between two heights in a near surface blended layer, and r_{ah} is the aerodynamic resistance to heat transport (s/m) between two heights.

To solve the iteration process, it is necessary to select hot and cold endmembers, a linear relationship between Ts and (dT) is assumed (Bastiaanssen et al., 1998a) (Eq. (7)), where a and b coefficients are empirically determined for each image.

$$dT = a + bT \quad (7)$$

The cold (wet) endmember candidates are selected in well-vegetated areas where H is assumed to be zero and maximum LE for a well-watered agricultural field at the full cover canopy, while for the hot (dry) endmember candidates the LE is assumed to be zero and maximum H for an agricultural field having no-green vegetation and dry soil surface layer. Usually, the cold endmember is selected within a set of candidates with the highest NDVI (5%), and the lowest Ts (20%) percentiles. Conversely, the hot endmember is selected based on the lowest NDVI (10%) and the highest Ts (20%) percentiles. Within geeSEBAL, these ranges are set as default (standard); however, the user can easily select other percentile values as input parameters according to hydrometeorological conditions, since the standard percentiles were calibrated and recommended for semiarid climates (Allen et al., 2013). In this study, we used the percentiles for cold pixels 5% (NDVI), 1% (Ts), and, hot pixels 1% (NDVI), 10% (Ts).

2.5. Field data of evapotranspiration - eddy covariance measurements

Modeled energy balance components and $ETa_{24\,h}$ were compared to measured data, provided by an eddy covariance flux tower installed in the field used to measure the micrometeorological variables and the energy balance components for estimating evapotranspiration covering the two ratoon seasons analyzed. The EC consists of a three-dimensional sonic anemometer and an infrared gas analyzer - IRGASON (Campbell Scientific, Logan, Utah, USA), positioned considering the prevailing wind direction, operated by a data logger (CR 3000, Campbell Scientific Instruments, Utah, USA) to record raw high-frequency data at 10 Hz.

The micrometeorological variables measured above the canopy were net radiation (CNR4, Net radiometer - Kipp & Zonen, Delft, Netherlands) and precipitation (CS700-L, Hydrological Services Pty. Ltd., Sydney, Australia). This equipment was positioned 5 m above the soil surface. On the ground, two soil heat flux plates were installed to measure the heat flow in the soil (HFP01-L, Campbell Scientific, Inc. Logan, Utah, USA). Low-frequency data were collected continuously at 5-second intervals averaging over 30 min. The raw data from the EC system (10 Hz) were processed using *EddyPro Advanced software* (LICOR, 2020a), and *Tovi software* (LICOR, 2020b) was used for data gap filling and flow partitioning every 30 min.

The flux data obtained over the two ratoons, on average showed an energy balance closure on a daily scale of about 77%, more details in Bispo (2020). In some cases, this results in a considerable amount of available energy (Rn - G) not being accounted for in the partitioning of latent and sensitive heat flux (λE + H), which could cause significant discrepancies in the comparisons with the results from remote sensing. The errors inherent in Rn (net radiation), λE (latent heat flux), H (sensitive heat flux), and G (heat flux in the soil) are reported as 5–10%, 15–20%, 15–20%, and 20–30%, respectively, according to (Foken, 2008; Vickers et al., 2010). For this reason, the Bowen Ratio values obtained with the flux tower data were used to adjust λE and H by forcing the closure following the procedure suggested by Twine et al. (2000). The λE values that represent the energy per unit area and per unit time were converted into evapotranspiration depth for each time interval and then 24 h-accumulated, resulting in actual daily evapotranspiration ($ETa_{24\,h}$). Also, an instantaneous evaporative fraction (EF) was estimated considering the energy available used by the plants (Rn – G) divided by the surface energy balance directly relates to evapotranspiration (λE).

To evaluate the effectiveness of geeSEBAL, the time series Python function was used by selecting the pixels over the upwind footprint to estimate instantaneous modeled energy balance components and $ET_{24\,h}$ from geeSEBAL, and the modeled data were compared to ground data (eddy flux tower). Daily crop coefficient (Kc) was estimated using daily geeSEBAL-$ETa_{24\,h}$ (satellite overpasses day), considering the entire sugarcane area, divided by ETo from the weather station following Eq. (8) (Allen et al., 1998), then Kc values from satellite overpasses day were interpolated using GDD to estimate daily Kc for the entire sugarcane season. With the daily Kc, it was possible to estimate daily ETa multiplying daily Kc to ETo. Crop water productivity (WP) was estimated by dividing the stalk yield (Kg per ha) by the modeled accumulated ETa for both growing seasons (Eq. (9)).

$$Kc = \frac{ETa}{ETo} \tag{8}$$

Where Kc is the crop coefficient; ETa is the actual daily evapotranspiration (mm); ETo is the reference evapotranspiration (mm).

$$WP = \frac{Yield}{ET} \tag{9}$$

Where WP is the crop water productivity (Kg/m^3) and ET is the total evapotranspiration in m^{-3} per ha.

After getting geeSEBAL-$ETa_{24\,h}$, the remote sensing-based soil water balance (RS-SWB) was calculated for each sugarcane season following Allen et al. (1998), considering the soil attributes data, soil water depletion fraction (p) adjusted based on ETc and effective rooting depth varying from 0.60 m (crop initial stage) to 0.80 m (crop late stage).

2.6. Statistical analysis

The energy balance components and the ETa estimated by geeSEBAL were compared with the data measured in the field through the EC flux tower. To measure the accuracy of the model, the R-square, RMSE (root mean squared error), and Bias indicators were applied according to Eqs. (10) and (11), respectively.

$$\mathrm{RMSE} = \sqrt{\sum_{i=1}^{n} \frac{(Y_i - \bar{Y}_i)^2}{n}} \tag{10}$$

Where RMSE is the root mean squared error; *n* is the sample size; Y is the observed variable; $\bar{Y}$ is the modeled variable.

$$Bias = \sum_{i=0}^{n} \frac{(Y_i - \bar{Y}_i)}{n} \tag{11}$$

Where *n* is the sample size; Y is the observed variable; $\bar{Y}$ is the modeled variable.

3. Results

Overall, the fourth and fifth growing seasons had similar average maximum and minimum temperatures equal to 30.9 ± 3.8 °C and 31.4 ± 3.6 °C for maximum temperature, and 18.2 ± 3.0 °C and 17.9 ± 3.7 °C for minimum temperature respectively, with temperature average equal to 24.6 °C for both seasons, 10.5% greater than the historical average for the region (23.3 °C) (Fig. 3).

Accumulated precipitation was 988 mm and 974 mm in the 4th and 5th ratoon seasons, respectively, on average 21% lower than the average historical amount of 1242 mm. For both ratoons, precipitation was irregular over the growing seasons, resulting in only 32 days and 31 days with precipitation over 10 mm respectively, distributed from October to February (rainy season).

3.1. geeSEBAL energy balance validation

Accord to Fig. 4, Rn, LE, H, ETa, and EF presented R^2 over 0.90 for all variables except G which was equal to 0.86. Also, except for G, all the EB components presented low RMSE and bias; however, despite the reasonable values of G, (9.2 W m^{-2}) and bias (−14.9 W m^{-2}), G values have little influence on EB because their values are considered very low, less than 5% of Rn in this study.

The Table 2 summarize the statistical indices for all modeled (geeSEBAL) and measured (flux tower) energy balance components and ETa.

3.2. Crop development and crop evapotranspiration

According to Fig. 5, the lowest SAVI values, considering Landsat 7 and Landsat 8 images, were 0.18 and 0.20 for the 4th and 5th ratoons respectively at the beginning of the respective crop seasons due to soil covered with sugarcane straw (post-harvest crop residues). After harvest, the SAVI values decrease to close to bare soil values around 0.12. The maximum SAVI value observed was 0.61 at 222 days after harvest (DAH) for the 4th ratoon and 0.60 at 169 DAH for the 5th ratoon. In this study, the SAVI values at harvest were 0.44 and 0.49 for the 4th and 5th ratoons, respectively.

For both growing seasons, SAVI values were similar and followed the development of the plants allowing the farmers to make decisions monitoring the crop stage such as the full cover stage at peak SAVI (both growing seasons in February) and the beginning of stalk maturity stage when SAVI start to decrease influenced by the reduction of green LAI. This occurred when SAVI reached about 0.50 (by May) and irrigation is cut-off to promote the concentration of carbohydrates in the stalks, and to improve the sugar and ethanol yields.

We observed that geeSEBAL accurately modeled the ETa values, represented spatially and temporally as shown in Fig. 6 (Landsat 8) for each crop development stage, and followed the SAVI values (Fig. 4). Therefore, low SAVI values a few days after harvesting presented also low ETa values, due to the low leaf area of the plants. However, as SAVI increases, ETa also increased until it reached its maximum value when

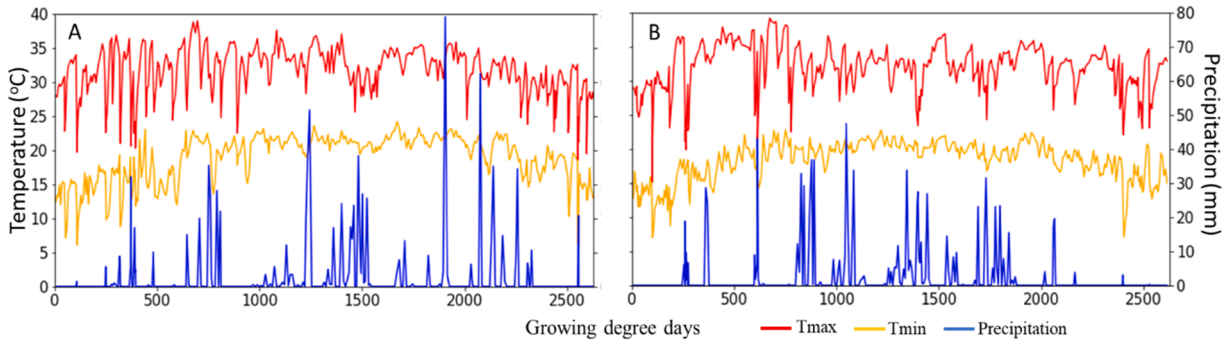

Fig. 3. Daily precipitation and daily maximum (Tmax) and minimum (Tmin) temperature over the 4th (A) and 5th (B) ratoon growing seasons.

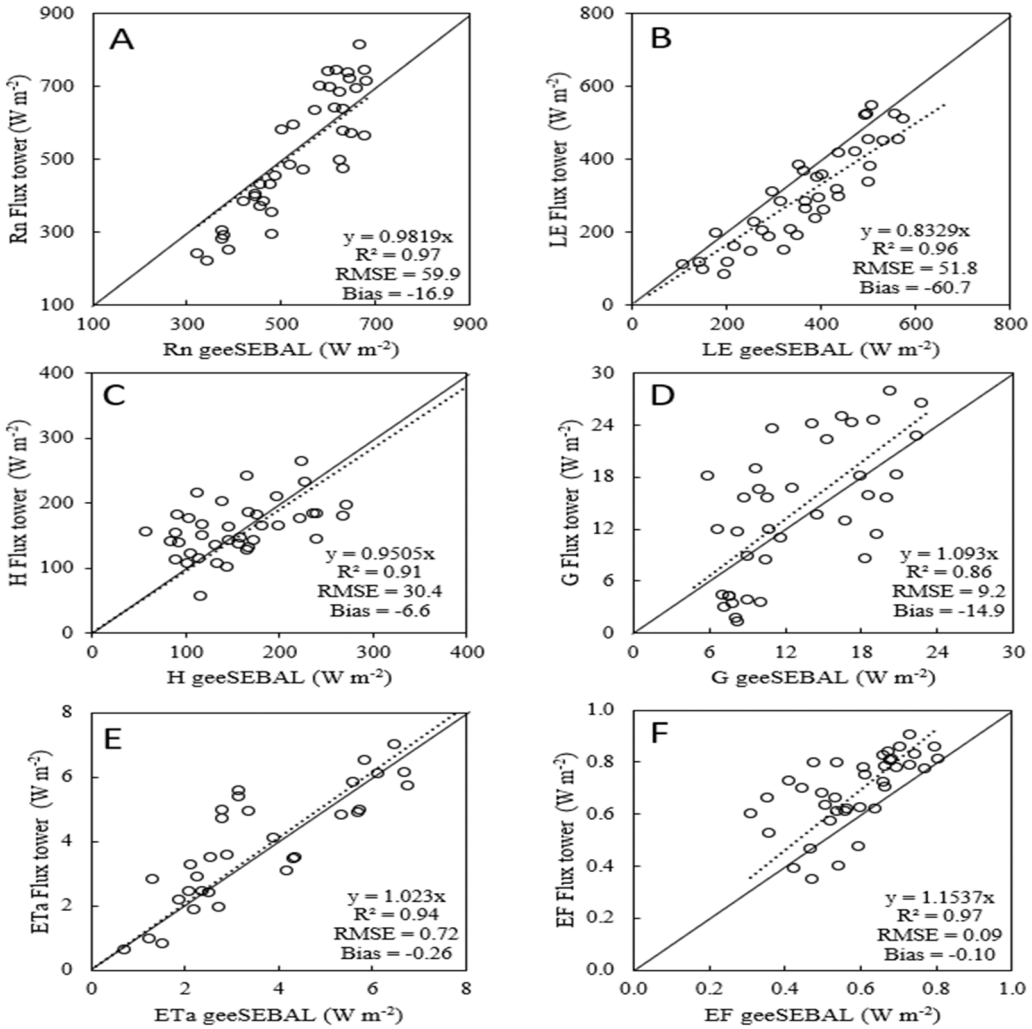

Fig. 4. Measured energy balance components and actual evapotranspiration by the Eddy Covariance flux tower method compared with the values modeled by the geeSEBAL. Rn: net radiation; LE: latent heat flux; H: sensible heat flux; G: soil heat flux; ETa: actual evapotranspiration; EF: instantaneous evaporative fraction.

plants reached maximum vegetation cover (SAVI greater than 55) at the beginning of the stalk maturation stage. Consequently, due to a decrease in SAVI values, the ETa also decreased as shown in Fig. 6 ($DAH_{4th} = 340$ and $DAH_{5th} = 337$).

The Kc values were modeled for each satellite overpass time using the ETa modeled from the geeSEBAL and the ETo values from the meteorological station (Fig. 7), with the Kc values plotted over the GDD of the ratoon's cycles, a Kc-GDD relationship is obtained, with an R^2 equal to 0.77 and 0.76 for the 4th and 5th growing seasons, following acceptably the Kc measured by the EC system. We noticed for the 5th ratoon, the modeled Kc values were slightly overestimated compared to daily measured data, mainly due to greater ETa variability at the late stage.

The results from modeled Kc values were extrapolated to the entire seasons based on the Kc-GDD relationship and daily evapotranspiration estimations (daily ETa were done and compared to measured data (Fig. 8). About the 4th ratoon, the data presented R^2 equal to 0.89, RMSE equal to 0.76, and less than 2% underestimating of ETa compared to de

Table 2
Summary of statistical indices used to evaluate the performance of the geeSEBAL compared to measure data (flux tower) at the field.

	Rn	LE	H	G	ETa	EF
RMSE	59.9	51.8	10.4	9.2	0.72	0.09
Bias	-16.9	-60.7	30.4	9.2	-0.26	-0.10
R^2	0.97	0.96	0.91	0.86	0.94	0.97

RMSE: Root mean squared error; R^2: R-square; Rn: net radiation; LE: latent heat flux; H: sensible heat flux; ETa: actual evapotranspiration; EF: evaporative fraction.

flux tower. Regarding the 5th ratoon, as modeled Kc values were overestimated, the results affected the modeled ETa and, on average, overestimating the evapotranspiration by about 15%; however, there was a low RMSE (0.62) and R^2 equal to 0.88. Maximum modeled daily Kc values were 1.12 and 1.14 for the 4th and 5th ratoon seasons and, on average 0.88 (4th ratoon) and 0.86 (5th ratoon), very close to the EC system for the 4th ratoon (0.86) and the 5th ratoon following the ETa values, the Kc from EC system was about 20% lower (Kc = 0.71).

Considering the two growing seasons as shown in Fig. 9, the ETa presented great results following the measured ETa by the EC and SAVI values, and the modeled accumulated ETa was 1266 mm and 1248 for the 4th and 5th ratoons respectively, representing water productivity of

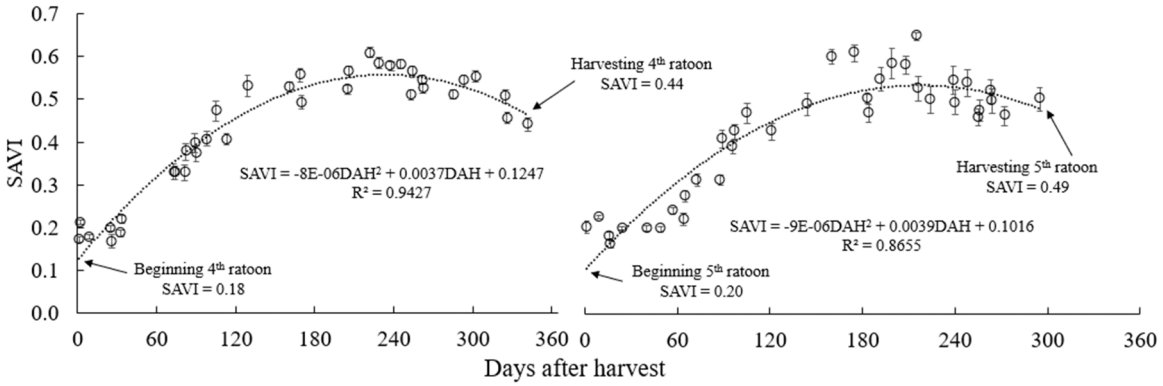

Fig. 5. Temporal evolution of the soil adjusted vegetation index (SAVI) values for sugarcane for the 4th and 5th growing seasons.

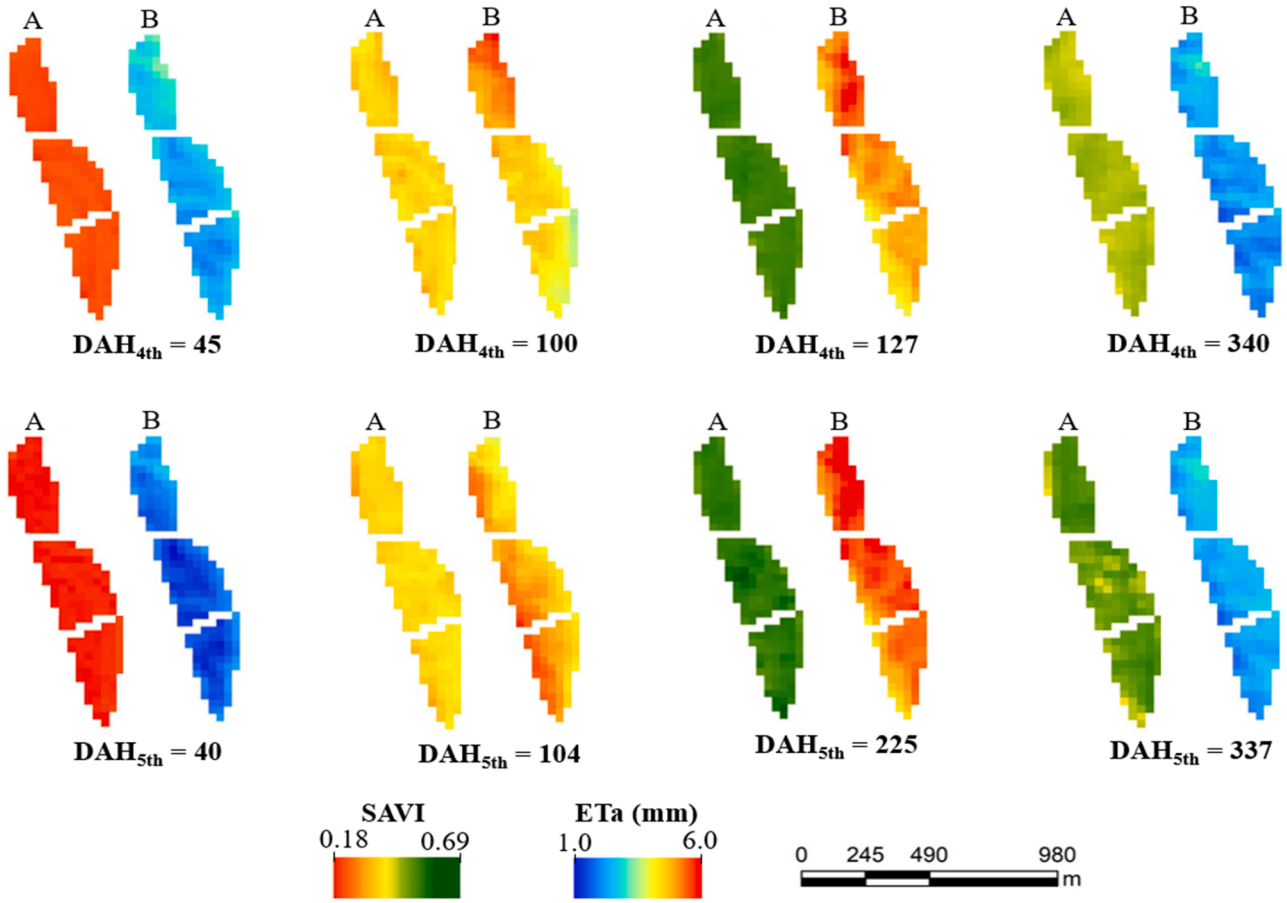

Fig. 6. Spatial and temporal distribution of soil adjusted vegetation index (SAVI) (A) and actual evapotranspiration (ETa) (B) as a function of the days after harvesting (DAH).

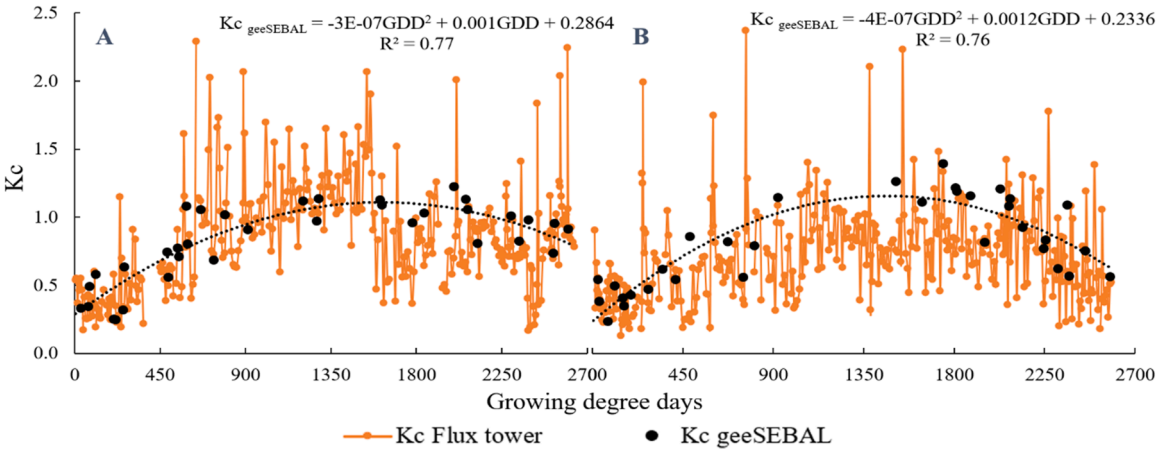

Fig. 7. Modeled and measured Kc values over the 4th (A) and 5th (B) ratoons. Kc: crop coefficient.

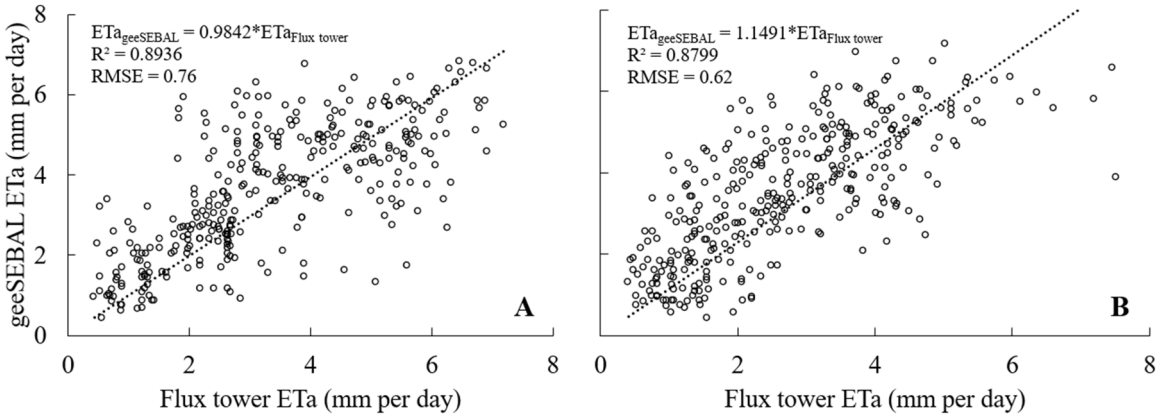

Fig. 8. Modeled and measured evapotranspiration values (ETa) comparison to the 4th (A) and 5th (B) ratoons.

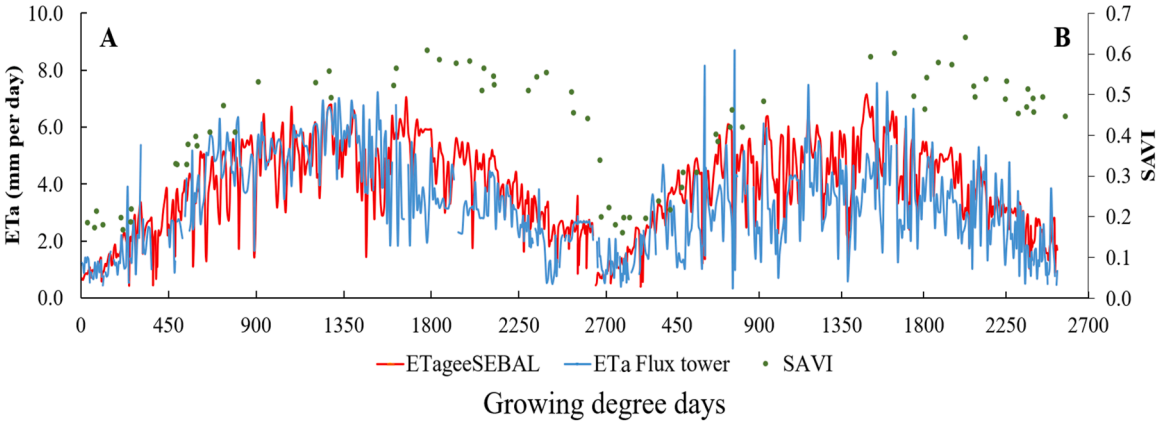

Fig. 9. Soil adjusted vegetation index (SAVI), modeled and measured evapotranspiration values (ETa) over the 4th (A) and 5th (B) ratoons.

10 and 9.7 kg m^{-3}. Overall, all the WP values were very similar between the growing seasons because the similar yields (127 and 121 Mg ha^{-1}), irrigation, precipitation, and ETo were very close between seasons.

So, an efficient way of increasing WP for sugarcane is through irrigation, increasing water supply to avoid water stress and ensure high stalk yields. In this study, there were increments of 58 and 52 Mg ha^{-1} greater than the national yield for the 4th and 5th ratoons respectively, after applying 584 and 560 mm of irrigation, i.e., an increase of 10 and 10.8 Mg per mm of water applied for each growing season. The ETa and Kc variability for each vegetative stage are summarized in Fig. 10.

3.3. *The remote sensing-based soil water balance*

With modeled ETa it was possible to estimate the RS-SWB for the two ratoon seasons (Fig. 11). We observed water stress occurring during the development stage of the crop and the irrigation system was not able to apply the required water demand which resulted in water stress for the plants for the 4th (total of 584 mm) and 5th (total of 560 mm) growing seasons.

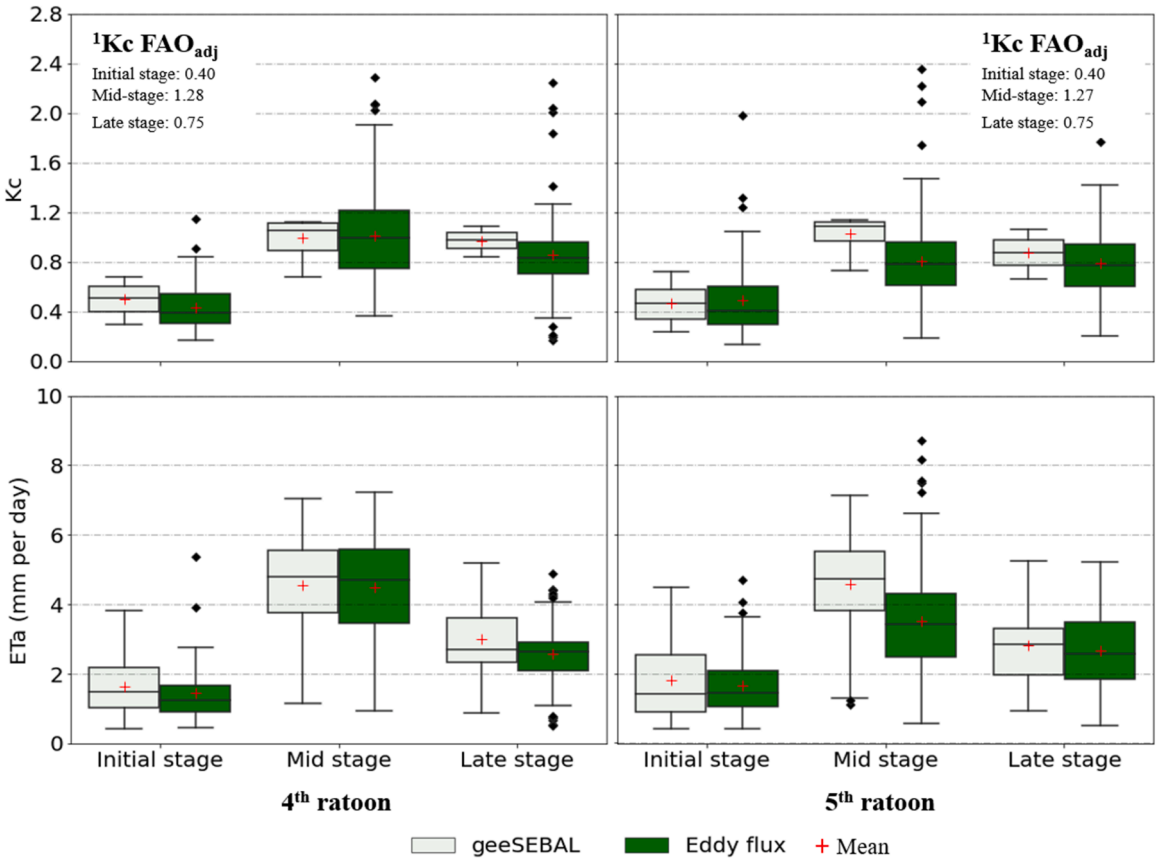

Fig. 10. Crop coefficient (Kc) and actual evapotranspiration (ETa) for initial, mid, and late vegetative stage for the 4th and 5th ratoons seasons. [1]Allen et al., (1998).

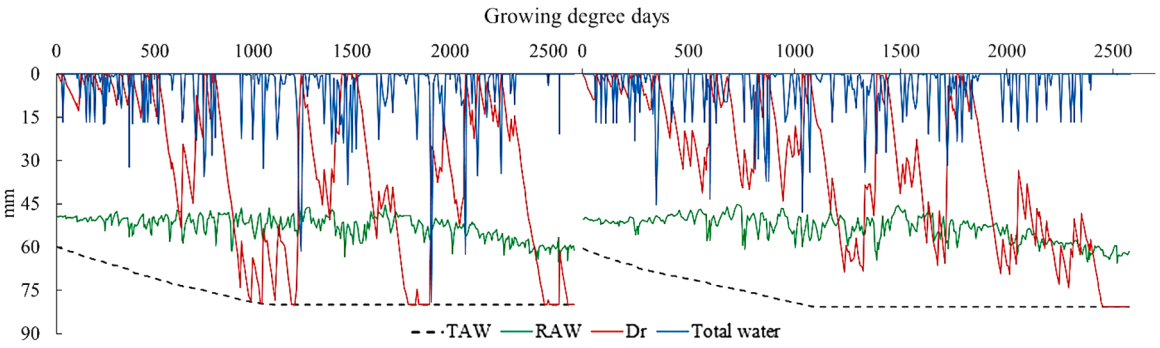

Fig. 11. Total water available (TAW), readily available water (RAW), depletion (Dr) over the 4th and 5th growing seasons based on growing degree days (GDD).

4. Discussion

Regarding the weather data for the two sugarcane growing seasons (Fig. 3), it was favorable to the sugarcane development because sugarcane requires high temperatures and humidity for reaching high yields, the minimum and maximum temperature must be between 20 °C and 35 °C (Marin et al., 2014; Vianna et al., 2020) which has occurred for almost the entire period of cultivation. Sugarcane in Brazil is purposefully planted in the dry season (June and July) to be harvested after one year during the dry season to increase the total recoverable sugar (TRS) concentration in the stalk, resulting in higher sugarcane quality and ability to be transformed into sugar or ethanol (Marin et al., 2021). Precipitation was poorly distributed during the evaluated period, requiring supplementation via irrigation, mainly during the regrowth stage (right after harvest). Irrigation is required mainly after harvesting to ensure the regrowth of the ratoons, and optimal stalk development until physiological maturity (Inman-Bamber et al., 1994), being essential to maintain proper soil water content in the root zone for attaining high yields.

The EB components and ETa values agreed very well with those measured by the EC system (Fig. 4). Despite the reasonable values of G, its values have little influence on EB because their values are considered very low, less than 5% of Rn in this study. According to Mukaka (2012), the EB components values shown in this study indicated the accurate performance of geeSEBAL, with similar results also observed by Yang et. al (2018) and Campos et. al. (2017).

SAVI values (Fig. 5), after reach the peak values (full cover) has its values decreased because of the maturation stage, the SAVI values decrease until harvest, due to the reduction in green leaf area index (LAI) which is expected in this stage as shown in Gonçalves et. al., (2017) and Silva et. al. (2012). Vegetation indices, such as SAVI, have been used to monitor irrigated sugarcane and other crops supporting

water management as described in Zhang et al. (2015), Venancio et al. (2020), and Campos et al. (2017). GeeSEBAL accurately modeled the ETa values spatially and over growing seasons (Fig. 6) for each crop development stage. As SAVI represents the vegetative vigor of the plants, we expect that any changes in SAVI values will impact the ETa values, because the increase or decrease in absorbed radiation in the visible red and near-infrared wavelengths by the leaves is directly related to the ability of plants to carry out their physiological activities properly, such as photosynthesis (Taiz et al., 2017). We observed in the late season for the 5th ratoon (337 DAH – Fig. 6), that SAVI values showed a high variability compared to the other periods, as shown in Fig. 5 (vertical bars). This was likely due to the high occurrence of damping-off caused by the association between the tall height of the plants (over 4 m) and high wind speed, also caused by the fact that the crop might not be senescing equally so there could be in-field variability in the SAVI due to different senescence rates.

Due to good agreement between modeled (geeSEBAL) and measured (flux tower) data, overall, the Kc values (Fig. 7) over growing seasons with high R^2 and similar to Allen et. al. (1998) and Marin et al. (2020) for the two ratoon seasons. The accumulated ETa presented great results following the measured ETa by the EC and SAVI values. Overall, all the WP values were very similar between the growing seasons because the similar yields (127 and 121 Mg ha^{-1}), irrigation, precipitation, and ETo were very close between seasons. These results were slightly lower than Leal et. al. (2017) and greater than Silva et. al. (2011), both conducted in Brazil. According to Teixeira et. al. (2016), WP ranged from 2.8 to 6.0 kg m^{-3} in a study in the state of São Paulo, much lower than our findings in this research (at least 40% lower), likely because in most of Brazil the sugarcane is not irrigated. Regarding the yield, both ratoons resulted in values greater than the expected Brazilian average for the next harvest (69 t ha^{-1}) (CONAB, 2021).

This approach, using only orbital data, through meteorological data from ERA5-Land presented satisfactory results of Kc and ETa with great potential to be used in areas cultivated with sugarcane for monitoring and irrigation management. Although the average modeled ETa values were greater than measured values for all the crop stages, the values were quite similar except for the 5th ratoon at mid-stage when modeled ETa was about 30% greater than measured values (Fig. 10). Consequently, Kc values presented the same performance. We notice that measured ETa and Kc presented greater variability than modeled values for both ratoon seasons, and many outlier values even to ETa. Regarding Kc FAO_{adj}, the values agreed to modeled and measured values for the initial stage for both ratoons when the ETa is still low; however, as atmosphere demand increased, this difference become higher, Kc FAO_{adj} reaching at mid-stage, 26% (EC system), and 23% (modeled) greater for the 4th ratoon respectively, 56% (EC system), and 23% (modeled) respectively for the 5th ratoon. There are many studies where irrigation ensured appropriate soil water content in the root zone and K_c values decreased under high atmosphere demand, i.e., high ETo values (Marin and Angelocci, 2011; Nassif et al., 2014; Marin et al., 2016, 2020). Crop canopies limit water loss by partially or completely closing the stomata under high evaporative demand, allowing the plants to maintain a favorable internal water balance even with optimum water content in the soil profile and high atmospheric demand for water (Boyer, 1982; Ciais et al., 2005; Franks, 2013; Vinya et. al, 2013).

The variability of the measured ETa (flux tower) in relation to modeled data (geeSEBAL) was also observed in Laipelt et al. (2021) analyzing data from different biomes and land use. Accord to the authors, the main challenge in developing a high resolution and large-scale product is the endmember selection for calibration and the definition of its domain area. The algorithm is highly sensitivity to the spatial domain, which can significantly change ET accuracy (Tang et al., 2013) when the selected endmembers present discrepant values (Long et al., 2011).

Both growing seasons showed some level of water stress after the crop reached the peak Kc (full cover phase) when the irrigation required was very high due to the low volume of precipitation and high evapotranspiration rates over the period (Fig. 11). The water stress was observed mainly during the final stages of growth for the 4th ratoon when the irrigation events are limited to increment the concentration of sugar in the stalks. The effects of soil water stress on crop ET reduces the Kc value. After the root zone depletion exceeds RAW is high enough to limit evapotranspiration to less than potential values and the Kc begins to decrease in proportion to the amount of water remaining in the root zone, consequently decreasing ET. Under rainfed conditions in low precipitation regions, due to the severe water stress over the growing seasons, the Kc values is reduced reducing the ETa and photosynthetic activity, as a result increasing the yield loss as observed in Gonçalves et al. (2017). However, the period of greatest susceptibility to water stress is the period of rapid crop development, when the plants already have a high leaf area index and need a greater volume of water to meet their physiological needs (Pires et al., 2008; Gonçalves et at, 2017). Also, sugarcane is relatively drought resistant, needing a long period of water stress to reduce the stalk's yield. (Ridesa, 2015). The current version of geeSEBAL uses Landsat images and state-of the-art global reanalysis data to estimate ET time series, thus showing promising results even for field-scale studies in data scarce areas. The use of surface energy balance algorithms like geeSEBAL and automated calibration algorithms like CIMEC in cloud computing environments, such as GEE), can provide new opportunities to improve water management for irrigated crops at high spatial resolution for long-term time series.

5. Conclusions

- This research was conducted in the largest sugarcane producing region of Brazil using an open-source SEBAL framework implemented within the Google Earth Engine (GEE) through the Application Programming Interface (API) to estimate evapotranspiration and water balance in the root system of a growing sugarcane field, considering two growing seasons (4th and 5th ratoons).
- The modeled EB components using the geeSEBAL model agreed well with the Eddy Covariance system values, considering both satellite overpass time and modeled ETa over growing seasons. Consequently, Kc values presented the same performance to measured and Allen et al. (1998).
- With modeled ETa over the seasons, it was possible to properly estimate the RS-SWB for the two ratoons identifying water stress for both seasons. WP obtained values that were similar between the seasons, with 10 and 9,7 kg m^{-3} for 4th and 5th respectively.
- Finally, the ET assessment showed the potential for geeSEBAL to improve water use for irrigation management for sugarcane in Brazil and mitigate the impacts of drought on stalk yields due to increasing water demand for food production and water supply. Given that geeSEBAL does not require any ground measurement as input, we anticipate that this tool may be useful for irrigated agriculture for field and regional-scale studies on water and energy balances, as well as for water resources management in missing climate data areas worldwide where this issue can be a challenge to properly estimate ET.

Declaration of Competing Interest

The authors declare that they have no known competing financial interests or personal relationships that could have appeared to influence the work reported in this paper.

Data availability

No data was used for the research described in the article.

Acknowledgments

The authors would like to gratefully acknowledge the Daugherty Water for Food Global Institute at the University of Nebraska for its scientific support. The financial support provided by the São Paulo Research Foundation (FAPESP grants 2020/08365–1; 2021/00720–0); the Brazilian Research Council (CNPq grants 425174/2018–2, 300916/2018–3 and 302597/2021–2), the Biosystems Engineering Laboratory at USP/ESALQ; the research group of the Institute of Hydraulic Research at UFRGS; and Irrigation and Drainage Laboratory at UNESP. The financial support provided by the Brazilian Agency for the Improvement of Higher Education (CAPES - Brazil) in partnership with the Brazilian National Water Agency (ANA - Brazil) is also acknowledged.

References

Allen, R., Pereira, L., Raes, D., Smith, M., 1998. FAO Irrigation and Drainage Paper. No. 56. Crop Evapotranspiration. Guidelines for computing crop water requirements. Crop Water Requir. Irrig. Drain. Pap. 56.

Allen, R.G., Tasumi, M., Trezza, R., 2007. Satellite-based energy balance for mapping evapotranspiration with internalized calibration (METRIC)—model. J. Irrig. Drain. Eng. 133, 380–394. https://doi.org/10.1061/(ASCE)0733-9437(2007)133:4(380).

Allen, R.G., Burnett, B., Kramber, W., Huntington, J., Kjaersgaard, J., Kilic, A., Kelly, C., Trezza, R., 2013. Automated calibration of the METRIC-landsat evapotranspiration process. JAWRA J. Am. Water Resour. Assoc. 49, 563–576, 10.1111/jawr.12056.

Anderson, M.C., Norman, J.M., Diak, G.R., Kustas, W.P., Mecikalski, J.R.A., 1997, two-source time-integrated model for estimating surface fluxes using thermal infrared remote sensing. Remote Sensing Environmental, [S.L.], v. 60, [S.N.], p. 195–216.

Bastiaanssen, W.G.M., Pelgrum, H., Wang, J., Ma, Y., Moreno, J.F., Roerink, G.J., van der Wal, T., 1998b, A remote sensing surface energy balance algorithm for land (SEBAL): 2. Validation. J. Hydrol. 212–213, 213–229. doi.org/10.1016/S0022–1694 (98) 00254–6.

Bastiaanssen, W.G.M., Menenti, M., Feddes, R.A., Holtslag, A.A.M., 1998a. A remote sensing surface energy balance algorithm for land (SEBAL): 1. Formulation. J. Hydrol. 212–213, 198–212. https://doi.org/10.1016/S0022-1694(98)00253-4.

Bastiaanssen, W.G.M., Noordman, E.J.M., Pelgrum, H., Davids, G., Thoreson, B.P., Allen, R.G., 2005. SEBAL model with remotely sensed data to improve waterresources management under actual field. Cond. J. Irrig. Drain. Eng. 131, 85–93. https://doi.org/10.1061/(ASCE)0733-9437(2005)131:1(85).

Bhattarai, N., Dougherty, M., Marzen, L.J., Kalin, L., 2012. Validation of evaporation estimates from a modified surface energy balance algorithm for land (SEBAL) model in the south-eastern United States. Remote Sens. Lett. 3, 511–519. https://doi.org/10.1080/01431161.2011.632655.

Bhattarai, N., Quackenbush, L.J., Im, J., Shaw, S.B., 2017, A new optimized algorithm for automating endmember pixel selection in the SEBAL and METRIC models. Remote Sens. Environ. 196, 178–192 https://doi.org/10.1016/j. rse.2017.05.009.

Bispo, R.C., 2020, Measurements and modeling of evapotranspiration in sugarcane in northwest São Paulo. Doctoral thesis, p.94, State University of São Paulo, Botucatu.

Bispo, R.C., Hernandez, F.B.T., Gonçalves, I.Z., Neale, C.M.U., Teixeira, A.H.C., 2022. Remote sensing based evapotranspiration modeling for sugarcane in Brazil using a hybrid approach. Agric. Water Manag. v. 271, 10776. https://doi.org/10.1016/j.agwat.2022.107763.

Boyer, J.S., 1982. Plant productivity and environment. Science 218, 443–448.

Campos, I., Balbontín, C., González-Piqueras, J., González-Dugo, M.P., Neale, C.M.U., Calera, A., 2016. Combining a water balance model with evapotranspiration measurements to estimate total available soil water in irrigated and rainfed vineyards. Agric. Water Manag., Amst. v. 165, 141–152.

Campos, I., Neale, C.M.U., Suyker, A., Arkebauer, T.J., Gonçalves, I.Z., 2017. Reflectance based crop coefficients REDUX: for operational evapotranspiration estimates in the age of high producing hybrid varieties. Agric. Water Manag., Amst. v. 187, 140–153.

Campos, I., Neale, C.M.U., Arkebauer, T.J., Suyker, A.E., Gonçalves, I.Z., 2018. Water productivity and crop yield: a simplified remote sensing driven operational approach. Agric. For. Meteorol., Amst. v. 249, 501–511.

Ciais, P., Reichstein, M., Viovy, N., Granier, A., Ogée, J., Allard, V., Aubinet, M., Buchmann, N., Bernhofer, C., Carrara, A., Chevallier, F., De Noblet, N., Friend, A.D., Friedlingstein, P., Grunwald, T., Heinesch, B., Keronen, P., Knohl, A., Krinner, G., Loustau, D., Manca, G., Matteucci, G., Miglietta, F., Ourcival, J.M., Papale, D., Pilegaard, K., Rambal, S., Seufert, G., Soussana, J.F., Sanz, M.J., Schulze, E.D., Vesala, T., Valentini, R., 2005. Europe-wide reduction in primary productivity caused by the heat and drought in 2003. Nature 437, 529–533.

Dijk, M.V., Morley, T., Rau, M.L., Saghai, Y., 2021. A meta-analysis of projected global food demand and population at risk of hunger for the period 2010–2050. Nat. Food 2, 494–501. https://doi.org/10.1038/s43016-021-00322-9.

Foga, S., Scaramuzza, P.L., Guo, S., Zhu, Z., Dilley, R.D., Beckmann, T., Schmidt, G.L., Dwyer, J.L., Joseph Hughes, M., Laue, B., 2017. Cloud detection algorithm comparison and validation for operational Landsat data products. Remote Sens. Environ. 194, 379–390. https://doi.org/10.1016/j.rse.2017.03.026.

Conab - Companhia Nacional de Abastecimento, 2021. Acompanhamento da safra brasileira: Cana-de-açúcar, safra 2021/2022, 3o levantamento. v.8, n.3 -. Terceiro levantamento, Brasília, p. 1–62, 2021.

Foken, T., 2008, The energy balance closure problem: an overview. Ecol. Appl. 18 (6), 1351e1367.

Foster, T., Gonçalves, I.Z.; Campos, I., Neale, C.M.U., Brozović, 2019, N. Assessing landscape scale heterogeneity in irrigation water use with remote sensing and in situ monitoring. Environmental Research Letters, v.14, n. 2, p. 40.

Franks, P.J., 2013. Passive and active stomatal control: either or both? N. Phytol. 198, 325–327.

Gonçalves, I.Z., Barbosa, E.A.A., Santos, L.N.S., Nazário, A.A., Feitosa, D.R.C., Tuta, N.F., Matsura, E.E., 2017. Water relations and productivity of sugarcane irrigated with domestic wastewater by subsurface drip. In: Agricultural Water Management, vol. 185. Elsevier,, pp. 105–115.

Hersbach, H., Bell, B., Berrisford, P., Hirahara, S., Horanyi, A., Munoz-Sabater, J., Nicolas, J., Peubey, C., Radu, R., Schepers, D., Simmons, A., Soci, C., Abdalla, S., Abellan, X., Balsamo, G., Bechtold, P., Biavati, G., Bidlot, J., Bonavita, M., De Chiara, G., Dahlgren, P., Dee, D., Diamantakis, M., Dragani, R., Flemming, J., Forbes, R., Fuentes, M., Geer, A., Haimberger, L., Healy, S., Hogan, R.J., Holm, E., Janiskova, M., Keeley, S., Laloyaux, P., Lopez, P., Lupu, C., Radnoti, G., de Rosnay, P., Rozum, I., Vamborg, F., Villaume, S., Thepaut, J.N., 2020. The ERA5 global reanalysis. Q. J. R. Meteorol. Soc. 146, 1999–2049. https://doi.org/10.1002/qj.3803.

Inman-Bamber, N.G., 1994. Temperature and seasonal effects on canopy development and light interception of sugarcane. Field Crops Res., V. 36, 41–51. https://doi.org/10.1016/0378-4290(94)90051-5.

Jaafar, H.H., Ahmad, F.A., 2019. Time series trends of Landsat-based ET using automated calibration in METRIC and SEBAL: The Bekaa Valley, Lebanon. Remote Sens. Environ. https://doi.org/10.1016/j.rse.2018.12.033.

Kayser, R.H., Ruhoff, A., Laipelt, L., de Mello Kich, E., Roberti, D.R., de Arruda Souza, V., Rubert, G.C.D., Collischonn, W., Neale, C.M.U., 2022. Assessing geeSEBAL automated calibration and meteorological reanalysis uncertainties to estimate evapotranspiration in subtropical humid climates. Agric. For. Meteorol. 314, 108775.

Laipelt, L., Kayser, R.H.B., Fleischmann, A.S., Ruhoff, A., Bastiaanssen, W., Erickon, T.A., Melton, F., 2021. Long-term monitoring of evapotranspiration using the SEBAL algorithm and Google Earth Engine cloud computing. J. Photogramm. Remote Sens. 178, 81–96.

Leal, D.P.V., Coelho, R.D., Barbosa, F.S., Júnior, E.F.F., Mauri, R., Santos, L.C., 2017. Water productivity for sugar and biomass of sugarcane varieties. Rev. Bras. Eng. Agríc. Ambent v. 2 (n), 9. https://doi.org/10.1590/1807-1929/agriambi.v21n9p618-622.

Licor, 2020a, Eddypro software instruction manual. V. 7. https://www.licor.com/documents/1ium2zmwm6hl36yz9bu4.

Licor, 2020b, Tovi user guide. V. 2.8. https://licor.app.boxenterprise.net/s/7t9z11sw53qg1qe4dhga84mwgvs3e8ni.

Long, D., Singh, V.P., Li, Z.-L., 2011, How sensitive is SEBAL to changes in input variables, domain size and satellite sensor? J. Geophys. Res. Atmos. 116 https://doi.org/10.1029/2011JD016542.

Marin, F., Ratallino-Edreira, J.I., Andrade, J., Grassini, P., 2021. Sugarcane yield and yield components as affected by harvest time. Sugar Tech. v. 100, 1–13.

Marin, F.R., Angelocci, L.R., 2011. Irrigation requirements and transpiration coupling to the atmosphere of a citrus orchard in Southern Brazil. Agric. Water Manag 98, 1091–1096. https://doi.org/10.1016/j.agwat.2011.02.002.

Marin, F.R., Ribeiro, R.V., Marchiori, P.E.R., 2014. How can crop modeling and plant physiology help to understand the plant responses to climate change? A case study with sugarcane. Theor. Exp. Plant Physiol. v. 26, 49–63.

Marin, F.R., Angelocci, L.R., Nassif, D.S.P., Costa, L.G., Vianna, M.S., Carvalho, K.S., 2016. Crop coefficient changes with reference evapotranspiration for highly canopy-atmosphere coupled crops. Agric. Water Manag 163, 139–145. https://doi.org/10.1016/j.agwat.2015.09.010.

Marin, F.R., Inman-Bamber, G., Silva, T.G.F., Nassif, D.F.P., Carvalho, K.S., 2020. Sugarcane evapotranspiration and irrigation requirements in tropical climates. Theor. Appl. Clim. 140, 1349–1357. https://doi.org/10.1007/s00704-020-03161-z.

Masek, J.G., Vermote, E.F., Saleous, N., Wolfe, R., Hall, F.G., Huemmrich, F., Gao, F., Kutler, J., Lim, T.K., 2006. A Landsat surface reflectance data set for North America, 1990-100. IEEE Geosci. Remote Sens. Lett. 3, 68–72.

Mecikalski, J.M., Diak, G.R., Anderson, M.C., Norman, J.M., 1999, Estimating fluxes on continental scales using remotely sensed data in an atmosphere-land exchange model. Journal of applied Meteorology, v. 38, [S.N.], p. 1352–1369.

Morton, C.G., Huntington, J.L., Pohll, G.M., Allen, R.G., McGwire, K.C., Bassett, S.D., 2013. Assessing calibration uncertainty and automation for estimating evapotranspiration from agricultural areas using METRIC. JAWRA. J. Am. Water Resour. Assoc. 49, 549–562. https://doi.org/10.1111/jawr.12054.

Mu, Q., Zhao, M., Running, S.W., 2011. Improvements to a MODIS global terrestrial evapotranspiration algorithm. Remote Sens. Environ. 115, 1781–1800. https://doi.org/10.1016/j.rse.2011.02.019.

Mukaka, M.M., 2012. Statistics corner: A guide to appropriate use of correlation coefficient in medical research. Malawi Med. J.: J. Med. Assoc. Malawi 24 (3), 69–71.

Munoz-Sabater, J., Dutra, E., Agustí-Panareda, A., Albergel, C., Arduini, G., Balsamo, G., Boussetta, S., Choulga, M., Harrigan, S., Hersbach, H., Martens, B., Miralles, D.G., Piles, M., Rodríguez-Fernandez, N.J., Zsoter, E., Buontempo, C., Thépaut, J.-N., 2021. ERA5-Land: A state-of-the-art global reanalysis dataset for land applications. Earth Syst. Sci. Data Discuss. 2021, 1–50. https://doi.org/10.5194/essd-2021-82.

Nassif, D.S.P., Marin, F.R., Costa, L.G., 2014. Evapotranspiration and transpiration coupling to the atmosphere of sugarcane in southern Brazil: scaling up from leaf to field. Sugar Tech. 16, 250–254. https://doi.org/10.1007/s12355-013-0267-0.

Neale, C.M.U., Bausch, W.C., Heerman, D.F., 1989. Development of reflectance-based crop coefficients for corn. Trans. ASAE v. 32, 1891–1899.
Norman, J.M., Kustas, W.P., Humes, K.S., 1995. A two-source approach for estimating soil and vegetation energy fluxes in observations of directional radiometric surface-temperature. Agric. For. Meteorol., Amst. v. 77 (n. 3–4), 263–293.
Norman, J.M., Anderson, M.C., Kustas, W.P., French, A.N., Mecikalski, J., Torn, R., Diak, G.R., Schmugge, T.J., Tanner, B.C.W., 2003. Remote sensing of surface energy fluxes at 101-m pixel resolutions. Water Resource. Research v. 39, 1221.
Peel, M.C., Finlayson, B.L., McMahon, T.A., 2007. Updated world map of the Köppen-Geiger climate classification. Hydrol. Earth Syst. Sci. 11, 1633–1644. https://doi.org/10.5194/hess-11-1633-2007.
Pires, R.C.M., Arruda, F.B., Sakai, E., 2008. Irrigação e drenagem. In: DINARDO-MIRANDA, L.L., VASCONCELOS, A.C.M., LANDELL, M.G.A. (Eds.), Cana-de-açúcar. Instituto Agronômico, Campinas, p. 882.
PRB – Population Reference Bureau, 2020, 2020 world population data sheet.
Ridesa, 2015. Rede Interuniversitária para o Desenvolvimento do Setor Sucroalcooleiro. 45 anos De. Var. rb De. cana-De. -açúcar 136p.
Ruhoff, A., Paz, A., Collischonn, W., Aragão, L., Rocha, H., Malhi, S., Y., 2012. A MODISbased energy balance to estimate evapotranspiration for clear-sky days in Brazilian tropical Savannas. Remote Sens. 4 (3), 703–725, 10.3390/ rs4030703.
Santos, H.G., Jacomine, P.K.T., Anjos, L.H.C., Oliveira, V.A., Lumbreras J.F., Coelho, M. R., Almeida, J.A., Filho A., J.C., Oliveira, J.B. de, Cunha, T.J.F. Brazilian agricultural research corporation. Brazilian soil classification system, 5 ed. Embrapa Soils, Brasília, p. 564, 2018.
Shuttleworth, W.J., 2012. Terrestrial Hydrometeorology, 1o. In: Wiley, John (Ed.), & Sons, Ltd, Chichester, UK. https://doi.org/10.1002/9781119951933.
Silva, V., Borges, C., Farias, C., Singh, V., Albuquerque, W., Silva, B., 2012. Water requirements and single and dual crop coefficients of sugarcane grown in a tropical region, Brazil. Agric. Sci. 3, 274–286. https://doi.org/10.4236/as.2012.32032.
Silva, T.G.F., Magna, S.B.M., Zolnier, S., Sores, J.M., Vieira, V.J.S., Gomes Júnior, W.F., 2011. Water requirement and efficiency of water use of irrigated sugarcane in semi-arid Brazil. Rev. bras. eng. agríc. ambient. https://doi.org/10.1590/S1415-43662011001200007.
Taiz, L., Zeiger, E., Moller, I.M., Murphy, A., 2017. Plant physiology and development. 6. Ed. Artmed. 761.
Tang, R., Li, Z.-L., Chen, K.-S., Jia, Y., Li, C., Sun, X., 2013. Spatial-scale effect on the SEBAL model for evapotranspiration estimation using remote sensing data. Agric. . Meteorol. 174–175, 28–42. https://doi.org/10.1016/j.agrformet.2013.01.008.
Teixeira, A.H.C., Leivas, J.F., Ronquim, C.C., Victoria, D.C., 2016. Sugarcane Water Productivity Assessments in the São Paulo state, Brazil. Int. J. Remote Sens. Appl. (IJRSA) V. 6. https://doi.org/10.14355/ijrsa.2016.06.009.
Twine, T.E., Kustas, W.P., Norman, J.M., Cook, D.R., Houser, P.R., Meyers, T.P., Prueger, J.H., Starks. P.J., Wesely, M.L., 2000, Correcting eddy-covariance flux underestimates over a grassland. Agricultural and Forest Meteorology, Amsterdam, v. 103, [S.N.], p. 279–300.
Venancio, L.P., Mantovani, E.C., Amaral, C.H., do., Neale, C.M.U., Gonçalves, I.Z., Filgueiras, R., Eugenio, F.C., 2020. Potential of using spectral vegetation indices for corn green biomass estimation based on their relationship with the photosynthetic vegetation sub-pixel fraction. Agric. Water Manag., V. 236. https://doi.org/10.1016/j.agwat.2020.106155.
Venancio, L.P., Mantovani, E.C., Amaral, C.H. do, Neale, C.M.U., Gonçalves, I.Z., Filgueiras, R., Campos, I., 2019. Forecasting corn yield at the farm level in Brazil based on the FAO-66 approach and soil-adjusted vegetation index (SAVI). Agricultural Water Management 225. https://doi.org/10.1016/j.agwat.2019.105779.
Vermote, E., Justice, C., Claverie, M., Franch, B., 2016. Preliminary analysis of the performance of the Landsat 8/OLI land surface reflectance product. Remote Sens. Environ. 185, 46–56.
Vianna, M., dos, S., Nassif, D.S.P., Dos Santos, C.K., Marin, F.R., 2020. Modelling the trash blanket effect on sugarcane growth and water use. Comput. Electron. Agric. v. 172, 105361.
Vickers, D., Gockede, M., Law, B.E., 2010. Uncertainty estimates for 1-h averaged turbulence fluxes of carbon dioxide, latent heat, and sensible heat. Tellus Ser. B Chem. Phys. Meteor. 62 (2), 87e99.
Vinya, R., Malhi, Y., Fisher, J.B., Brown, N., Brodribb, T., Aragão, L.E.O.C., 2013. Xylem cavitation vulnerability influences tree species' habitat preferences in miombo woodlands. Oecologia 173, 711–720.
Wagle, P., Bhattarai, N., Gowda, P.H., Kakani, V.G., 2017. Performance of five surface energy balance models for estimating daily evapotranspiration in high biomass sorghum. ISPRS J. Photogramm. Remote Sens. 128, 192–203. https://doi.org/10.1016/j.isprsjprs.2017.03.022.
Yang, Y., Shang, S., Jiang, L., 2012. Remote sensing temporal and spatial patterns of evapotranspiration and the responses to water management in a large irrigation district of North China. Agric. For. Meteorol. 164, 112–122, 10.1016/j.agrformet.2012.05.011.
Yang, Y., Martha, C., Anderson, F.G., Brian, W., Christopher, R.H., Jason, A.O., Joseph, A., Yun, Y., Liang, S., Wayne, D., 2018. Field-scale mapping of evaporative stress indicators of crop yield: An application over Mead, NE, USA. Remote Sens. Environ., V. 210, 387–402. https://doi.org/10.1016/j.rse.2018.02.020.
Zhang, H., Anderson, R.G., Wang, Dong, 2015. Satellite-based crop coefficient and regional water use estimates for Hawaiian sugarcane. Field Crops Res. 180, 143–154. https://doi.org/10.1016/j.fcr.2015.05.023.
Zhang, K., Kimball, J.S., Running, S.W., 2016. A review of remote sensing based actual evapotranspiration estimation. Wiley Interdiscip. Rev. Water 3, 834–853, 10.1002/wat2.1168.